Published in final edited form as:
Am J Physiol Heart Circ Physiol. 2005 May ; 288(5): H2077–H2087. doi:10.1152/ajpheart.00526.2003.

The Molecular Correlates of Altered Expression of Potassium Currents in Failing Rabbit Myocardium

Jochen Rose, MD[*], **Antonis A Armoundas, PhD**[*], **Yanli Tian, MD**, **Deborah DiSilvestre, BS**, **Miroslava Burysek, BS**, **Victoria Halperin**, **Brian O'Rourke, PhD**, **David A. Kass, MD**, **Eduardo Marbán, MD, PhD**, and **Gordon F. Tomaselli, MD**

Abstract

Action potential (AP) prolongation is a hallmark of failing myocardium. Functional down regulation of K currents is a prominent feature of cells isolated from failing ventricles. The detailed changes in K current expression differ depending upon the species, the region of the heart and the mechanism of induction of heart failure. We used complementary approaches to study K current down regulation in pacing-tachycardia induced heart failure in the rabbit. The APD at 90% repolarization was significantly longer in cells isolated from failing hearts compared to controls (539 ± 162 ms failing versus 394 ± 114 control, $p < 0.05$). The major K currents in the rabbit heart, I_{K1}, I_{to} and I_K were functionally down regulated in cells isolated from failing ventricles. The mRNA levels of Kv4.2, Kv1.4, KChIP2 and Kir2.1 were significantly down regulated, while the Kv4.3, Erg, KvLQT1 and minK were unaltered in the failing compared with the control left ventricles. Significant down regulation in the long splice variant of Kv4.3 but not total Kv4.3, Kv4.2 and KChIP2 immunoreactive protein was observed in cells isolated from the failing ventricle with no change Kv1.4, KvLQT1, and in Kir2.1 immunoreactive protein levels. Multiple cellular and molecular mechanisms underlie the down regulation of K currents in the failing rabbit ventricle.

Keywords

I_{to}; I_{K1}; I_K; action potential; heart failure; rabbit

Introduction

Congestive heart failure is a major cause of mortality worldwide, with up to 50% of affected patients dying suddenly (12). Ventricular arrhythmias are a common cause of sudden death in heart failure patients (44), however, the underlying mechanism of these arrhythmias is poorly understood (34). Action potential (AP) prolongation is a hallmark of failing ventricular myocardium (5,24) and prolongation, particularly if it is heterogeneous, can predispose to exaggerated dispersion of repolarization and non-excitable gap reentry (14). AP prolongation in-and-of itself is arrhythmogenic; longer APs may be associated with repolarization abnormalities such as afterdepolarizations, which can predispose to triggered arrhythmias (35).

Functional down regulation of K currents is a recurring theme in hypertrophied and failing ventricular myocardium. However, the specific changes in K current expression differ depending on the species and the model of heart failure (4). A reduction in the density of I_{to} is

Correspondence to: Gordon F. Tomaselli, M.D., Johns Hopkins University, Division of Cardiology, 844 Ross Building, 720 Rutland Avenue, Baltimore, MD 21205, Phone: (410) 955-2776, Fax: (410) 955-7953, E- mail: E-mail: gtomasel@jhmi.edu .
[*]These authors contributed equally to this work

the most consistent ionic current change in cardiac hypertrophy and failure but down regulation of I_{K1} (5,24), I_{Kr} and I_{Ks} (46) densities have also been described.

The molecular basis of the differences in K current density in the failing heart is not clear but is likely to be multifactorial. In an effort to better understand the fundamental mechanisms of K current down regulation in the failing heart we studied the ionic currents in ventricular myocytes isolated from control rabbits and those with pacing-induced heart failure. We correlated K current densities with mRNA and immunoreactive protein levels encoding the major K channel subunits expressed in rabbit ventricle. Similar to previous reports (46) we found a reduction in I_{to} (encoded by Kv4.3, Kv4.2, and KChIP2), I_K (encoded by Erg, KvLQT1 and minK) and I_{K1} (encoded by Kir2.1) densities in cells isolated from failing compared to control hearts. The reduction in I_{to} density observed was associated with a decrease in Kv4.2, KChIP2 and Kv4.3 long splice variant but not total immunoreactive protein. The decreased functional expression of I_{K1} was associated with a significant change in the level of the Kir2.1 mRNA without a significant change in the total immunoreactive protein. On the other hand the decreased functional expression of I_K was not associated with a significant change in KvLQT1, minK and Erg mRNA or KvLQT1 and minK immunoreactive protein.

Methods

Pacing-induced heart failure model

New Zealand white rabbits of either sex underwent sterile implantation of a bipolar pacing system. Rabbits were anesthetized with intravenous thiopental sodium, intubated and volume ventilated. A laparotomy was performed and the diaphragm and pericardium were opened to expose the heart. Two custom-made pacing wires were sutured to the apex of the heart. A VVI pacemaker (Minix 8340 or Thera SR 8962, Medtronic) was inserted into a pocket formed between the abdominal muscles. Rapid pacing was maintained by permanently attaching a magnet to the posterior surface of the pulse generator. Animals were allowed to fully recover for 3 to 4 days, after which pacing was initiated at 400 ppm for 2 to 4 weeks. Left ventricular dysfunction was verified by transthoracic echocardiography. All hemodynamic measurements were made with the pacemaker turned off. After 20 ± 4 days of pacing the left ventricular end-diastolic diameter was significantly increased and systolic fractional shortening (in % of end-diastolic diameter) was decreased (Table 1). In a randomly selected subset of rabbits, a Millar catheter was advanced via the right carotid artery into the left ventricle. The left ventricular pressure was recorded and its first derivative was calculated (dP/dt). The left ventricular end-diastolic pressure in failing hearts was significantly higher than in control hearts, while the left ventricular peak positive pressure tended to decrease. The maximum dP/dt was significantly lower in failing hearts as compared to control hearts (Table 1). These echocardiographic and hemodynamic findings are consistent with severe heart failure as were the physical findings of pleural effusions and ascites in the paced animals that were absent in controls (41). Sham operations were performed in three animals (n=3) and since electrophysiological data showed no significant differences from controls that did not undergo the sham operation, data from sham and unoperated control animals were pooled. All procedures involving the animals were approved the Institutional Animal Care and Use Committee of the Johns Hopkins University.

Isolation of ventricular myocytes

Isolated myocytes were obtained from 11 failing and 25 control hearts by enzymatic dissociation as previously described (30). In brief, hearts were quickly excised from rabbits anesthetized with pentobarbital. The left ventricular apex was removed for RNA and protein studies (see below) and the ventriculotomy was closed. The heart then was mounted on a Langendorff apparatus and perfused with a modified Krebs-Henseleit (KH) solution composed of (in mmol/L): NaCl 119, KCl 5, $MgSO_4$ 1, $NaHCO_3$ 25, KH_2PO_4 1, $CaCl_2$ 2, and glucose

10, followed by nominally Ca^{2+}-free KH and finally Ca^{2+}-free KH with collagenase (0.8 mg/mL, type II, Worthington). All perfusates were bubbled with 95% O_2/5% CO_2, maintained at 37°C and the flow rate was adjusted to maintain a perfusion pressure of approximately 75 mmHg. The hearts were removed from the perfusion apparatus, and the atria, the right ventricle, and the papillary muscles trimmed away. In a subset of control hearts (N=10), the subendocardial and subepicardial layers (less than 1 mm thick) of the left ventricle were isolated and the rest of the left ventricular wall is referred to as the midmyocardial layer, although this was the most heterogeneous preparation containing cells from all layers of the heart. All three layers were minced and incubated in a shaking 37°C bath for another 10 minutes in collagenase-containing solution. Cells were then filtered through a nylon mesh and stored at room temperature in the Krebs buffer containing 1 mmol/L Ca^{2+} for up to seven hours. Only Ca^{2+}-tolerant rod-shaped cells with clear cross striations and without spontaneous contractions or granulations were selected for experiments.

Electrophysiological recordings

All electrophysiological recordings were performed in myocytes from the mid-myocardial layer of the left ventricular free-wall unless otherwise is indicated.

The external solution for AP measurements contained (in mmol/L) NaCl 138, KCl 4, $CaCl_2$ 2, $MgCl_2$ 1, glucose 10, NaH_2PO_4 0.33, and N-(2-Hydroxyethyl)piperazine-N′-(2-ethanesulfonic acid) (HEPES) 10 (pH 7.4 with NaOH). For the recording of I_{to} only, 0.3 mmol/L $CdCl_2$ was added to the bath solution. The pipette solution for recording APs and I_{to} contained (in mmol/L) KCl 140, NaCl 5, $MgCl_2$ 1, HEPES 10, Ethylene glycol-bis-(2-aminoethyl)-N,N,N', N'-tetraacetic acid (EGTA) 2, and Mg- Adenosine 5'-triphosphate (ATP) 4, pH 7.4.

The external solution for I_K recordings contained (in mmol/L) NMG 140, KCL 5.4, $CaCl_2$ 0.1, $MgCl_2$ 1, $CdCl_2$ 0.5, glucose 10, HEPES 10 (pH 7.4 with NaOH). The pipette solution for I_{K1} and I_K recordings contained (in mmol/L) K-glutamate 120, KCl 10, $MgCl_2$ 2, HEPES 10, EGTA 5, Mg-ATP 2, and QX314 5 pH 7 .4. I_{K1} was blocked by superfusion with 2 mmol/L $BaCl_2$.

Whole-cell currents were recorded using an Axopatch 200A amplifier (Axon Instruments). Cell capacitance was calculated by integrating the area under an uncompensated capacity transient elicited by a 20-mV depolarizing pulse from a holding potential of −80 mV. Whole-cell currents were low-pass-filtered at 1 kHz and digitized at 5 kHz via a Digidata 1200 A/D (Axon Instruments) interface for off-line analysis. The data were analyzed using custom-written software.

APs were recorded at a rate of 0.5 Hz at 37°C, steady-state typically developed after five cardiac cycles. In all protocols AP data represent at least ten cardiac cycles under steady-state conditions. A square wave current pulse of 2 mec duration at 50% above the threshold was used to elicit action potentials.

I_{K1} and I_{to} were studied at room temperature. I_{K1} was elicited from a holding potential of −20 mV by voltage steps of 500 ms from −150 mV to +50 mV in 10 mV increments every 6 seconds. This protocol was repeated in the presence of 2 mmol/L $BaCl_2$ and I_{K1} is given as the Ba-sensitive current. I_{to} was elicited from a holding potential of −80 mV by voltage steps of 500 ms from −40 mV to +80 mV in 10 mV increments every 6 seconds. Standard pulse protocols were used to assay the biophysical properties of I_{to}. The protocols designed to elucidate the impact of variations in I_{to} on the AP were performed exclusively in cells from control hearts. In these hearts, cells were isolated from the subendocardial, midmyocardial and the subepicardial layers of the left ventricle.

I_K was studied at 37°C and was elicited from a holding potential of −50 mV by voltage steps of 3 s from −40 mV to +80 mV in 10 mV increments of 10 seconds.

mRNA analysis

The steady-state levels of mRNA, reflect the balance between transcription and degradation and were measured by either ribonuclease protection assay (RPA) or kinetic real-time PCR (RT-PCR) using left ventricular apical myocardium.

Preparation of cRNA probes—The DNA fragments used to generate rabbit-specific riboprobes were amplified from reverse-transcribed total rabbit ventricular RNA using the polymerase chain reaction (PCR). The PCR products were cloned into pCR2.1 (Invitrogen) and, if necessary, subcloned into the *EcoR1*-site of pSP70 (Promega). The region spanning the forward and reverse primers was cloned into pBS SK^- and the probe was transcribed using the T3 promoter. All constructs were confirmed by DNA sequencing (310 Genetic Analyzer, Perkin Elmer). The Na^+ channel template was designed to protect a fragment in the I-II linker of the Na^+ channel unique to the cardiac isoform, so that this is a myocyte-specific probe. The rabbit cardiac Na^+-channel (H1) probe spans nucleotides 1655 to 1801 (146 bp) and is shown in Table 2.

Ribonuclease protection assay—Total RNA was prepared using TRIzol reagent (Life Technologies) according to the manufacturer's instruction. The integrity of all RNA samples was confirmed by analysis on a denaturing agarose gel and quantified by optical density measurements at 260 nm. Ribonuclease protection assays were performed as described previously (15,23). The probes contained regions of the plasmid sequence at one end of the transcript, permitting easy distinction between any remaining undigested probe and the shorter, specifically protected region of the probe. Ten μg of yeast tRNA was used as a negative control to test for the presence of probe self-protection. Determinations were performed in duplicate on 10 μg of RNA from each ventricular sample.

Steady-state mRNA levels were quantified by exposing the gels on a storage phosphor screen, then scanning on a phosphoimager (Molecular Dynamics); quantification of the transcript levels was performed using ImageQuant software (Molecular Dynamics). The level of gene expression is given by the relative density of the protected fragment normalized to the density of the control protected fragment, the rabbit cardiac Na channel (H1), thereby normalizing for both RNA loading and the fraction of the sample that is derived from cardiac myocytes. This value was normalized to a reference sample to permit comparison among protection assays.

Real-time PCR—Fluorescence-based kinetic real-time PCR was performed using a Perkin-Elmer Applied Biosystems Model 7900 sequence-detection system. Total RNA was isolated from the rabbit ventricle using the Qiagen RNeasy kit with on-column DNase digestion. The 5′ nuclease activity of Taq DNA polymerase cleaves the probe, and a fluorescent signal is generated that is proportional to the amount of starting target template. Each reporter signal is then divided by the fluorescence of an internal reference dye (ROX) to normalize for non–PCR-related fluorescence and to the 18S RNA level. All primers and probes were synthesized by Applied Biosystems (Foster City, CA) and are shown in Table 2. The KChIP2 sequence was obtained by PCR amplification using the following primer pair: (5' TTGTCGGTGATTCTTCGGGGAA 3') and (5' CTAGATGACATTGTCAAAGAGC 3').

The level of gene expression was normalized to a reference sample to permit comparison among samples.

Protein analysis

Western blots were performed on tissue lysates from rapidly frozen ventricular tissue, as previously described (33). Proteins were separated on non-gradient gels between 7.5 and 15% acrylamide, depending upon the specific channel subunit to be measured. The same protein sample from a control heart was run on every gel and used as a reference for normalization across gels and expression of the housekeeping gene GAPDH was used to verify uniform protein loading and transfer.

Commercially available and custom-made primary antibodies to potassium channel subunits were used. Antibodies to Kv4.3 (AB5194; human) and Kv4.2 (AB5360; rat), were purchased from Chemicon (Temecula, CA) and the anti-Kv1.4 antibody (APC007; rat) from Alomone. Anti-ERG antibodies from both Chemicon (AB5908) and Alomone (APC062) exhibited high background and lack of specificity for ERG in rabbit ventricle and heterologously expressed HERG. A custom-made antibody was generated that recognizes the long splice variant of Kv4.3 (human) using the 19 amino-acid insert in this variant (27). The polyclonal antibody to KChIP2S/T (human) was raised to an epitope, SYDQLTDSVDDE, that spans the splice excision site in KChIP2 and is present in KChIP2S and 2T (13). The polyclonal antibody to KChIP2 has been previously described (2,13). The anti-KvLQT1 antibody (human) was generated by immunization of rabbits with conjugated peptides with the sequence DPPEERRLDHFSVDGYDSSVRK. Custom-made antibodies to Kir2.1 directed against the epitope LHGDLDASKESKAC (AA109–122), which is 100% homologous among the rabbit, dog and human, were generated in the chicken (Covance Research Products Inc.; Dublin, PA). Affinity purified IgY from egg yolks was used as the primary antibody and anti-chicken IgY as the secondary antibody (Affinity Bioreagents; Golden, CO) in Kir2.1 western blots.

Chemiluminescent detection was performed using hyperfilm-ECL (Amersham Life Science) after incubation with an anti-IgG horseradish peroxidase secondary antibody. The exposed film was digitally scanned and band densities were quantified using ImageQuant software (Molecular Dynamics). The amount of immunoreactive protein was quantified as the density of all specific bands normalized to GAPDH for protein loading this ratio was normalized by the density of the same reference sample run on every gel to facilitate comparisons across gels. The variability of the signal from the duplicate determinations was mandated to be less than 15%.

Statistical analysis

Pooled data are presented as mean ± SD or SEM. Statistical comparisons were made using an unpaired t-test. Linear regressions were compared by an analysis of covariance. A p value less than 0.05 was considered statistically significant.

Results

We studied 25 control and 11 pacing-induced (20 ± 4 days) heart failure rabbits and their hemodynamic characteristics are presented in Table 1. The hemodynamic data including an increase in left ventricular end diastolic volume, a marked reduction in fractional shortening and a dramatic reduction in the dP/dt_{max} are consistent with severe systolic dysfunction in the paced animals. In all animals heart weight and lung weight to body weight ratios were significantly increased (Table 1).

Action potential duration and K current densities in control and failing myocardium

Representative AP recordings in ventricular myocytes isolated from the midmyocardial layer of control and failing hearts are shown in Figure 1A. While the resting membrane potential was unchanged (data not shown), the APD is longer in the myocyte isolated from the failing

heart compared with that isolated from the control heart. The APD_{90} was significantly longer in cells isolated from failing compared to control ventricles (Fig. 1B; 17 cells isolated from 12 control and 12 cells from 5 failing ventricles; control 394±114 msec versus failing 539±162 ms, $p < 0.05$).

I_{K1} is the principal determinant of the resting membrane potential and is important in phase 3 repolarization. The inward I_{K1} density was significantly reduced in cells isolated from failing as compared to normal hearts at voltages more hyperpolarized than −90 mV (Fig. 2A–C). The rate of activation and the time course of current decay at negative voltages did not differ in cells isolated from control and failing hearts (Fig. 2A and Fig. 2B). The small outward component of I_{K1} was also reduced, but this did not reach statistical significance (Fig. 2D). The finding that the most significant changes in I_{K1} are at very negative voltages (I_{K1} is only modestly reduced at voltages near the resting membrane potential (V_m)), is consistent with the absence of a difference in V_m in cells isolated from control and failing hearts.

The most consistent current alteration in ventricular myocytes from failing hearts is a reduction in the density of I_{to}. This current was decreased by ~60% in cells isolated from failing hearts as compared to normal hearts (Fig. 3A–C). The reduction of I_{to} density was not a consequence of altered I_{to} voltage dependence or kinetics. The voltage dependencies of activation and steady-state inactivation (Fig. 3D) were unchanged as were the kinetics of current decay (Fig. 3E) in cells isolated from failing compared to cells from control hearts. Apparent differences in current density may, in principal, result from changes in the recovery from inactivation. The recovery of I_{to} in cells from both control and failing ventricles were best fit by a bi-exponential function (Fig. 3F). Neither the time constants nor the fraction of the more slowly recovering current component were different in cells isolated from control and failing hearts. Thus, the decrease in I_{to} density is best explained by a decreased number of functional channels in the membrane (24).

The delayed rectifier K currents are important components of the ventricular repolarization machinery. We measured the composite I_K current in mid left ventricular myocytes isolated from control and failing hearts. In Tyrode's solution with 10 mM KCl we consistently observed robust step and tail currents (Fig. 4B). Figure 4B shows that the step current, measured at the end of the 3 sec pulse, is significantly reduced at negative voltages in cells isolated from failing compared control myocardium. The peak tail current is significantly reduced in cells isolated from failing heart over the entire voltage range.

Correlation between native I_{to} density and action potential duration—The role that I_{to} plays in controlling the APD varies in different species, we correlated the density of I_{to} with the APD under different experimental conditions to better understand the role of this current in determining the APD in rabbit ventricular myocytes. Figure 5A shows APs and I_{to} currents at +60 mV from myocytes isolated from the subendocardial and subepicardial regions of the left ventricle. Myocytes from the subendocardium were characterized by a relatively long APD and a moderate I_{to} density. The myocytes isolated from the subepicardium were characterized by a shorter AP and a high I_{to} density but without a notch-and-dome morphology. In the 20 cells studied, there was an inverse correlation between I_{to} density and APD; the higher the I_{to} density the shorter the APD (Fig. 5B).

mRNA in control and failing hearts

The steady-state levels of total Kv4.3, Kv4.3L (long splice variant), Kv4.3S (short splice variant), Kv4.2, Kv1.4, KChiP2, Erg, KVLQT1, minK and Kir2.1 mRNA were measured by either RPA or kinetic RT-PCR.

Figure 6A shows a representative RPA for the Kir2 family of channel genes, Kir2.1 but not Kir2.2 or Kir2.3 was detected in rabbit ventricle while all three isoforms were present in brain. When normalized to the mRNA level for cardiac Na channel (Nav1.5) there is a significant decrease in steady-state levels of Kir2.1 mRNA in failing compared to control rabbit ventricle (Fig. 6B).

The Kv4 and KChIP2 genes underlie ventricular I_{to}, while Kv1.4 is thought to be a component of I_{to} in rabbit atrium (50) and in the endocardium of the ventricle in some species (52). The steady-state mRNA level of Kv4.3, Kv4.3L and Kv4.3S were not different in the failing compared to the control ventricle, while Kv4.2 and Kv1.4 were down regulated. KChIP2 primers were designed to hybridize to the 3' end of the molecule and therefore should recognize all KChIP2 variants found in other species. We found that, KChIP2 mRNA was significantly down regulated in the failing heart (Fig. 6C). In contrast, mRNA levels encoding subunits of the delayed rectifier current, KvLQT1, minK and Erg were unaltered in the failing versus control rabbit left ventricle.

Protein expression in control and failing hearts

We measured the steady-state levels of immunoreactive proteins in tissues isolated from the same hearts in which current recordings and mRNA measurements were made to gain insight into the underlying mechanism of K current down regulation in the failing heart. Figure 7 shows representative Western blots together with summary data for each channel subunit. The specificity of the bands for each of the channel subunits was determined by competition with the peptide epitope and/or the absence of reactivity with pre-immune serum.

There was a statistically significant down regulation of the Kv4.2 and the long splice variant Kv4.3 immunoreactive proteins, while we saw no significant change of the total Kv4.3 or Kv1.4. The KChIP2 splice variants run between 25 and 35 kDa (13). Total KChIP2 levels were significantly down regulated in failing ventricular myocardium, while splice variants containing the amino-terminal insert recognized by the anti-KChIP2S/T antibody were unchanged. There was no significant change in KvLQT1 immunoreactive protein in the failing heart samples compared with controls. Unlike proteins isolated from canine and human hearts, a specific band identifying minK at 15 kDa was not observed in rabbit ventricular myocardium. There was no significant change in the Kir2.1 immunoreactive protein (55 kDa) in the failing heart (Fig. 7C).

Discussion

Our data demonstrate prolongation of the APD in left ventricular myocytes isolated from severely failing compared to normal rabbit ventricles (Table 1), similar to that reported previously (41,46). The AP was prolonged significantly at 90% repolarization and was associated with a reduction in the density of I_{to} by ~60%, I_{K1} by ~50% (at voltages negative to E_K), and I_K by ~35%.

Our I_{to} data are in agreement with several previous reports in human (5,51), canine (24,28) and rabbit (41,46) left ventricular myocytes. Several notable exceptions are studies of compensated hypertrophy which were associated with either no change (8,47) or an increase in I_{to} density (29). The variance in detail regarding basal current densities and changes in heart failure may be due to differences in specific models or regions of the left ventricle from which the myocytes were isolated.

The molecular mechanism of I_{to} down regulation in structural heart disease is likely to be multifactorial. It has been argued that divergent gene products may underlie I_{to} in different regions of the heart (e.g. Kv4 vs. Kv1.4). In rabbit atria (50), Kv1.4 plays a prominent role in

the formation of I_{to}, however our data are consistent with the preponderance of evidence that supports the hypothesis that the Kv4 family of genes are the major contributors to the formation of I_{to} in the mammalian ventricle (15–17,22). Intriguingly, Kv1.4 mRNA has been found in the ventricle in a number of species and even increases in abundance in heart failure (7). Indeed, Kv1.4 (*KCNA4*) mRNA and protein are expressed in the rabbit ventricle but the level of protein is unchanged in the failing heart; similar to studies in human heart failure (23). Moreover, the biophysical features of I_{to} in cells isolated from normal or failing hearts, do not suggest a role for Kv1.4 in rabbit ventricular I_{to} (36).

The specific Kv4 family member that underlies I_{to} may differ depending upon the species. In humans and dogs it appears that Kv4.3 (*KCND3*) exclusively is the pore-forming subunit (16). In the rat, both Kv4.2 (*KCND2*) and Kv4.3 are expressed and it is the transmural expression of Kv4.2 that appears to vary (15). It has been argued that KChIP2 is the key determinant of I_{to} density across the wall of the mammalian heart and indeed a steep mRNA gradient exists (13,39). The role of KChIP2 in controlling the regional density of I_{to} in the ventricle is uncertain. Our data suggest that alterations in the expression of Kv4.2, and to a lesser extent KChIP2, underlie the down regulation of I_{to} in the failing rabbit ventricle (Figure 6 and Figure 7). Both the long and short splice variant of Kv4.3 (27) are expressed in the rabbit ventricle, the significance of the dramatic reduction in the immunoreactive long splice variant is uncertain.

I_{K1} density has been reported to increase (26), decrease (8) or remain unchanged (1,9,42,48) in the hypertrophied heart. Similar inconsistencies have been observed in pacing tachycardia models: reduced I_{K1} density has been seen in the dog (24), while unchanged current density was found in the rabbit (37,41,46). In human heart failure, reduced I_{K1} density was associated with no change in the steady-state level of Kir2.1 mRNA in failing compared to control hearts (23). We found no significant expression of Kir2.2 and Kir2.3 mRNA (Fig. 6A) in the rabbit ventricle similar to results in the canine heart (32). In contrast to the human studies, we found that the decreased I_{K1} density is associated with a modest but significant reduction in the level of the Kir2.1 mRNA without a significant change at the protein level.

Studies of the delayed rectifier K currents in hypertrophic and failing hearts are more limited and measurements of mRNA and protein levels of the I_K subunits are scarce. Myocytes from hypertrophied cat (18,19) and dog (47) ventricles exhibit a reduction in the density of one or both of the components of I_K while other studies of cells isolated from pressure-overload guinea pig (1,42) or spontaneously hypertensive rat (8) ventricles demonstrate no change in I_K. In the tachycardia pacing-induced heart failure model in the rabbit (46), both I_{Kr} and I_{Ks} were significantly smaller than those in control hearts, while in the analogous canine model I_{Ks} was significantly reduced (28) without a significant change in the voltage dependence or kinetics of the currents. The decreased functional expression of I_K in this study was not associated with a significant change in KvLQT1, minK and Erg mRNA or KvLQT1 and minK immunoreactive protein, similar to our previous studies of hErg in human HF (23), but distinct from another report of a decrease in KvLQT1 mRNA in failing compared to control human hearts (11). In contrast, in the chronic AV block-induced hypertrophy model in the dog, minK but not KvLQT1 mRNA was decreased, while both immunoreactive minK and KvLQT1 were significantly down regulated in the hypertrophied ventricle (38).

In summary, I_{to}, I_{K1} and I_K are functionally down regulated in the failing rabbit ventricle and the molecular basis of the current reduction varies for each of the currents. These data, in the context of the findings in other models of cardiac hypertrophy and failure, highlight the complexity of ion channel regulation in structural heart disease. The reduction in mRNA levels of Kv4.2 and KChIP2 may result from a change in the balance between transcription and mRNA degradation that suggests the possibility of transcriptional regulation of the subunits

encoding I_{to} in the failing heart, but the precise molecular mechanism is unknown. In the case of the other K channel subunits, steady-state levels of mRNA are not altered yet the level of immunoreactive protein may change (Kv4.3L) and current density may change without a significant change mRNA or immunoreactive protein levels of the relevant subunits (I_{K1}, I_K). The complexity of electrical remodeling in the failing heart is further exaggerated by other mechanisms of post-translational mo dulation of channel function. Such mechanisms include altered subcellular localization of channel proteins, modified subunit interactions such as has been observed between KCNE2 and KCNE3 and KvLQT1 (43,45) and altered neurohumoral signaling, for example the effect of β-adrenergic stimulation on I_{Ks} (31,49). The diversity of mechanisms that are associated with alterations the electrophysiology in the failing heart suggest that ion channels are down stream effectors of a number of interacting signaling pathways.

Mechanisms of action potential prolongation

The reduction in K current densities differentially contributes to the APD prolongation in pacing-induced heart failure in the rabbit. The outward component of I_{K1}, at voltages positive to E_K (Fig. 3C) contributes to phase 3 repolarization. Therefore, a reduction of I_{K1} density should prolong the termina l phases of the AP. The density of the I_K is significantly reduced in cells isolated from failing ventricular myocardium suggesting an important role for delayed rectifier currents in controlling ventricular repolarization (1,42). Although direct data are limited, mutations in I_K-encoding genes in the long QT syndrome (25) and the effects of drugs with class III antiarrhythmic action are compelling evidence for the importance of I_{Kr} and I_{Ks} in ventricular repolarization in the human heart.

In contrast, I_{to} is brief and there are no specific inhibitors of this current thus its role in setting the APD in larger animals and humans remains controversial. Most of the studies examining I_{to} in heart failure have used Ca^{2+}-buffered internal solutions, thus distorting any possible role of calcium-dependent processes. Under these conditions, several lines of evidence suggest that I_{to} can significantly influence the overall APD (5,21,24,40). Nevertheless, it is not clear whether this conclusion would also apply under more physiological conditions. Indeed, simulations employing the canine left ventricular myocyte model suggest that at physiological densities I_{to} has little effect on the APD. It is only when the current density is increased to levels that mimic those observed in rodents that the current significantly shortens the APD (3,20). Thus I_{to} may play a different role in repolarization of the rabbit ventricular myocyte compared with other species such as the dog and human.

In this and other models of heart failure reduced I_{to} density is associated with prolongation of the APD ((5,24) and Fig 5B). The correlation between I_{to} density and APD does not imply causality indeed the correlation coefficient of the regression line in figure 5B is only 0.64, indicating that other factors are involved in the regulation of the APD in this model. For example, by setting the plateau potential, I_{to} affects many downstream membrane currents like L-type Ca-current (20), delayed rectifier currents, and the Na^+-Ca^{2+} exchanger current.

Limitations of the study

A significant limitation of this study is that the comparison of currents, transcripts and proteins are by their nature correlative and do not prove participation of subunits in the generation of a given current. Indeed, we can not state with certainty that any change in a channel subunit is the proximate cause of the alteration in a given ionic current, indeed it is possible that a change in some other regulatory molecule, that we did not measure, produced the change in current. However, an important first step understanding the molecular basis of remodeling in HF is the characterization of the changes in channel subunit mRNA and protein that are known to underlie specific ionic currents.

The intracellular Ca^{2+} concentration was buffered in the present study by EGTA to reproduce the experimental conditions of previous studies (5,24) thus altering several membrane currents. Buffering intracellular Ca^{2+} will impact the crosstalk that occurs between cell surface membrane currents and intracellular Ca^{2+} homeostatic mechanisms (33,53). Calcium-induced inactivation of the L-type calcium channel is attenuated, slowing the current decay. The calcium-dependent transient outward chloride current (I_{to2}), if present, is probably completely blocked and the Na^{+}-Ca^{2+} exchange current is reduced (6).

The cells used in this study were all obtained from the left ventricular free wall while the tissues used for mRNA and protein measurements were from the apex of the heart. We cannot exclude regional differences in mRNA, protein and current expression in heart failure. In addition, we chose to confine our current measurements to cells isolated from a single transmural section of the left ventricle to avoid the confounding influence of baseline differences in current density that have been described in normal hearts (3,10,47). This highlights a general limitation of studies in which electrophysiological measurements are made on isolated myocytes from one region of the heart and molecular biological and protein chemical studies are done on another region.

The absence of a change in the level of immunoreactive protein on a Western blot does not exclude the possibility of a different subcellular distribution of the channel proteins with an alteration in the expression of surface membrane expression. Because of limitations in the amount tissue available for analysis in any given animal we chose not to perform the Western blots on membrane fractions.

Acknowledgements

This study was supported by a grant from the National Institutes of Health (P50 HL52307), AHA Mid-Atlantic Consortium (S98711M, GFT), by a fellowship from the Deutsche Forschungsgemeinschaft (Ro 1231/2-1 and 2-2, JR), and by an American Heart Association Beginning Grant-in-Aid (#0365304U, AAA).

References

1. Ahmmed GU, Dong PH, Song G, Ball NA, Xu Y, Walsh RA, Chiamvimonvat N. Changes in Ca(2+) cycling proteins underlie cardiac action potential prolongation in a pressure-overloaded guinea pig model with cardiac hypertrophy and failure. Circ Res 2000;86:558–570. [PubMed: 10720418]
2. An WF, Bowlby MR, Betty M, Cao J, Ling HP, Mendoza G, Hinson JW, Mattsson KI, Strassle BW, Trimmer JS, Rhodes KJ. Modulation of A-type potassium channels by a family of calcium sensors. Nature 2000;403:553–556. [PubMed: 10676964]
3. Antzelevitch C, Sicouri S, Litovsky SH, Lukas A, Kishnan SC, Di Diego JM, Gintant GA, Liu D-W. Heterogeneity within the ventricular wall Electrophysiology and pharmacology of epicardial, endocardial, and M cells. Circ Res 1991;69:1427–1449. [PubMed: 1659499]
4. Armoundas AA, Wu R, Juang G, Marban E, Tomaselli GF. Electrical and structural remodeling of the failing ventricle. Pharmacol Ther 2001;92:213–230. [PubMed: 11916538]
5. Beuckelmann DJ, Nabauer M, Erdmann E. Alterations of K+ currents in isolated human ventricular myocytes from patients with terminal heart failure. Circ Res 1993;73:379–385. [PubMed: 8330380]
6. Beuckelmann DJ, Wier WG. Sodium-calcium exchange in guinea-pig cardiac cells: exchange current and changes in intracellular Ca^{2+} J Physiol (Lond) 1989;414:499–520. [PubMed: 2607439]
7. Bodi I, Muth JN, Hahn HS, Petrashevskaya NN, Rubio M, Koch SE, Varadi G, Schwartz A. Electrical remodeling in hearts from a calcium-dependent mouse model of hypertrophy and failure: complex nature of K+ current changes and action potential duration. J Am Coll Cardiol 2003;41:1611–1622. [PubMed: 12742305]
8. Brooksby P, Levi AJ, Jones JV. The electrophysiological characteristics of hypertrophied ventricular myocytes from the spontaneously hypertensive rat. Journal of Hypertension 1993;11:611–622. [PubMed: 8397240]

9. Cerbai E, Barbieri M, Li Q, Mugelli A. Ionic basis of action potential prolongation of hypertrophied cardiac myocytes isolated from hypertensive rats of different ages. Cardiovasc Res 1994;28:1180–1187. [PubMed: 7954620]
10. Cheng J, Kamiya K, Kodama I, Toyama J. Differential effects of MS-551 and E-4031 on action potentials and the delayed rectifier K+ current in rabbit ventricular myocytes. Cardiovasc Res 1996;31:963–974. [PubMed: 8759253]
11. Choy A-M, Kuperschmidt S, Lang CC, Pierson RN, Roden DM. Regional expression of HERG and KvLQT1 in heart failure. Circulation 1996;94:164.
12. Cohn JN, Archibald DG, Ziesche S, Franciosa JA, Harston WE, Tristani FE, Dunkman WB, Jacobs W, Francis GS, Flohr KH, et al. Effect of vasodilator therapy on mortality in chronic congestive heart failure. Results of a Veterans Administration Cooperative Study. N Engl J Med 1986;314:1547–1552. [PubMed: 3520315]
13. Deschenes I, DiSilvestre D, Juang GJ, Wu Rc, An WF, Tomaselli GF. Regulation of Kv4.3 current by KChIP2 splice variants: a component of native cardiac I(to)? Circulation 2002;106:423–429. [PubMed: 12135940]
14. Di Diego JM, Antzelevitch C. High $[Ca^{2+}]_o$-induced electrical heterogeneity and extrasystolic activity in isolated canine ventricular epicardium. Phase 2 reentry. Circulation 1994;89:1839–1850. [PubMed: 7511994]
15. Dixon JE, McKinnon D. Quantitative analysis of potassium channel mRNA expression in atrial and ventricular muscle of rats. Circ Res 1994;75:252–260. [PubMed: 8033339]
16. Dixon JE, Shi W, Wang H-S, McDonald C, Yu H, Wymore RS, Cohen I, McKinnon D. Role of Kv4.3 K^+ channel in ventricular muscle A molecular correlate for the transient outward current. Circ Res 1996;79:659–668. [PubMed: 8831489]
17. Fiset C, Clark RB, Shimoni Y, Giles WR. *Shal*-type channels contribute to the Ca^{2+}-independent transient outward K^+ current in rat ventricle. Journal of Physiology 1997;500:51–64. [PubMed: 9097932]
18. Furukawa T, Bassett AL, Furukawa N, Kimura S, Myerburg RJ. The ionic mechanism of reperfusion-induced early afterdepolarizations in feline left ventricular hypertrophy. J Clin Invest 1993;91:1521–1531. [PubMed: 8386189]
19. Furukawa T, Myerburg RJ, Furukawa N, Kimura S, Bassett AL. Metabolic inhibition of ICa,L and IK differs in feline left ventricular hypertrophy. Am J Physiol 1994;266:H1121–H1131. [PubMed: 8160815]
20. Greenstein JL, Wu R, Po S, Tomaselli GF, Winslow RL. Role of the calcium-independent transient outward current I(to1) in shaping action potential morphology and duration. Circ Res 2000;87:1026–1033. [PubMed: 11090548]
21. Hoppe UC, Johns DC, Marban E, O'Rourke B. Manipulation of cellular excitability by cell fusion: effects of rapid introduction of transient outward K+ current on the guinea pig action potential. Circ Res 1999;84:964–972. [PubMed: 10222344]
22. Johns DC, Nuss HB, Marban E. Suppression of neuronal and cardiac transient outward currents by viral gene transfer of dominant-negative Kv4.2 constructs. J Biol Chem 1997;272:31598–31603. [PubMed: 9395498]
23. Kääb S, Dixon J, Duc J, Ashen MD, Näbauer M, Beuckelmann DJ, McKinnon D, Tomaselli GF. Molecular basis of transient outward current downregulation in human heart failure: A decrease in Kv4.3 mRNA correlates with a reduction in current density. Circulation 1998;98:1383–1393. [PubMed: 9760292]
24. Kääb S, Nuss HB, Chiamvimonvat N, O'Rourke B, Pak PH, Kass DA, Marban E, Tomaselli GF. Ionic mechanism of action potential prolongation in ventricular myocytes from dogs with pacing induced heart failure. Circ Res 1996;78:262–273. [PubMed: 8575070]
25. Keating MT, Sanguinetti MC. Molecular genetic insights into cardiovascular disease. Science 1996;272:681–685. [PubMed: 8614827]
26. Kleimann RB, Houser RS. Outward currents in normal and hypertrophied feline ventricular myocytes. Am J Physiol 1989;266:H1738–H1745.

27. Kong W, Po S, Yamagishi T, Ashen MD, Stetten G, Tomaselli GF. Isolation and characterization of the human gene encoding Ito: further diversity by alternative mRNA splicing. Am J Physiol 1998;275:H1963–H1970. [PubMed: 9843794]
28. Li GR, Lau CP, Ducharme A, Tardif JC, Nattel S. Transmural action potential and ionic current remodeling in ventricles of failing canine hearts. Am J Physiol Heart Circ Physiol 2002;283:H1031–H1041. [PubMed: 12181133]
29. Li Q, Keung EC. Effects of myocardial hypertrophy on transient outward current. Am J Physiol 1994;266:H1738–H1745. [PubMed: 8203574]
30. Liu Y, Gao WD, O'Rourke B, Marban E. Synergistic modulation of ATP-sensitive K^+ currents by protein kinase C and Adenosine Implications for ischemic preconditioning. Circ Res 1996;78:443–454. [PubMed: 8593703]
31. Marx SO, Kurokawa J, Reiken S, Motoike H, D'Armiento J, Marks AR, Kass RS. Requirement of a macromolecular signaling complex for beta adrenergic receptor modulation of the KCNQ1-KCNE1 potassium channel. Science 2002;295:496–499. [PubMed: 11799244]
32. Melnyk P, Zhang L, Shrier A, Nattel S. Differential distribution of Kir2.1 and Kir2.3 subunits in canine atrium and ventricle. Am J Physiol Heart Circ Physiol 2002;283:H1123–H1133. [PubMed: 12181143]
33. O'Rourke B, Peng LF, Kääb S, Tunin R, Tomaselli GF, Marban E. Mechanisms of altered exciation-contraction coupling in canine tachycardia-induced heart failure I: Experimental studies. Circ Res 1999;84:562–570. [PubMed: 10082478]
34. Packer M. Lack of relation between ventricular arrhythmias and sudden death in patients with chronic heart failure. Circulation 1992;85:I50–I56. [PubMed: 1728505]
35. Pak PH, Nuss HB, Tunin RS, Kääb S, Tomaselli GF, Marban E, Kass DA. Repolarization abnormalities, arrhythmias and sudden death in canine tachycardia-induced cardiomyopathy. J Am Coll Cardiol 1997;30:576–584. [PubMed: 9247535]
36. Po S, Roberds S, Snyders DJ, Tamkun MM, Bennett PB. Heteromultimeric assembly of human potassium channels. Molecular basis of a transient outward current? Circ Res 1993;72:1326–1336. [PubMed: 8495559]
37. Pogwizd SM, Schlotthauer K, Li L, Yuan W, Bers DM. Arrhythmogenesis and contractile dysfunction in heart failure: Roles of sodium-calcium exchange, inward rectifier potassium current, and residual beta-adrenergic responsiveness. Circ Res 2001;88:1159–1167. [PubMed: 11397782]
38. Ramakers C, Vos MA, Doevendans PA, Schoenmakers M, Wu YS, Scicchitano S, Iodice A, Thomas GP, Antzelevitch C, Dumaine R. Coordinated down-regulation of KCNQ1 and KCNE1 expression contributes to reduction of I(Ks) in canine hypertrophied hearts. Cardiovasc Res 2003;57:486–496. [PubMed: 12566121]
39. Rosati B, Pan Z, Lypen S, Wang HS, Cohen I, Dixon JE, McKinnon D. Regulation of KChIP2 potassium channel beta subunit gene expression underlies the gradient of transient outward current in canine and human ventricle. J Physiol 2001;533:119–125. [PubMed: 11351020]
40. Rozanski GJ, Xu L, Zhang K, Patel KP. Altered ionic currents of ventricular myocytes in rats with experimental heart failure. Am J Physiol. 1997
41. Rozanski GJ, Xu Z, Whitney RT, Murakami H, Zucker IH. Electrophysiology of rabbit ventricular myocytes following sustained rapid ventricular pacing. J Mol Cell Cardiol 1997;29:721–732. [PubMed: 9140829]
42. Ryder KO, Bryant SM, Hart G. Membrane current changes in left ventricular myocytes isolated from guinea pigs after abdominal aortic coarctation. Cardiovascular Research 1993;27:1278–1287. [PubMed: 8252589]
43. Schroeder BC, Waldegger S, Fehr S, Bleich M, Warth R, Greger R, Jentsch TJ. A constitutively open potassium channel formed by KCNQ1 and KCNE3. Nature 2000;403:196–199. [PubMed: 10646604]
44. Stevenson WG, Stevenson LW, Middlekauff HR, Saxon LA. Sudden death prevention in patients with advanced ventricular dysfunction. Circulation 1993;88:2953–2961. [PubMed: 8252708]
45. Tinel N, Diochot S, Lauritzen I, Barhanin J, Lazdunski M, Borsotto M. M-type KCNQ2-KCNQ3 potassium channels are modulated by the KCNE2 subunit. FEBS Lett 2000;480:137–141. [PubMed: 11034315]

46. Tsuji Y, Opthof T, Kamiya K, Yasui K, Liu W, Lu Z, Kodama I. Pacing-induced heart failure causes a reduction of delayed rectifier potassium currents along with decreases in calcium and transient outward currents in rabbit ventricle. Cardiovasc Res 2000;48:300–309. [PubMed: 11054476]
47. Volders PG, Sipido KR, Vos MA, Spatjens RL, Leunissen JD, Carmeliet E, Wellens HJ. Downregulation of delayed rectifier K(+) currents in dogs with chronic complete atrioventricular block and acquired torsades de pointes. Circulation 1999;100:2455–2461. [PubMed: 10595960]
48. Volders PGA, Sipido KR, Carmeliet E, Spatjens R, Vos MA. Repolarizing K+ currents Ito1 and IKs are larger in the right than the left ventricular midmyocardium of the dog. Circulation 1998;98:I–611.
49. Walsh KB, Kass RS. Regulation of a heart potassium channel by protein kinase A and C. Science 1988;242:67–69. [PubMed: 2845575]
50. Wang Z, Feng J, Shi H, Pond A, Nerbonne JM, Nattel S. Potential molecular basis of different physiological properties of the transient outward K+ current in rabbit and human atrial myocytes. Circ Res 1999;84:551–561. [PubMed: 10082477]
51. Wettwer E, Amos GJ, Posival H, Ravens U. Transient outward current in human ventricular myocytes of subepicardial and subendocardial origin. Circ Res 1994;75:473–482. [PubMed: 8062421]
52. Wickenden AD, Kaprielian R, Parker TG, Jones OT, Backx PH. Effects of development and thyroid hormone on K^+ currents and K^+ channel gene expression in rat ventricle. J Physiol 1997;504:271–286. [PubMed: 9365903]
53. Winslow RL, Rice J, Jafri S, Marban E, O'Rourke B. Mechanisms of altered excitation-contraction coupling in canine tachycardia-induced heart failure, II: model studies. Circ Res 1999;84:571–586. [PubMed: 10082479]

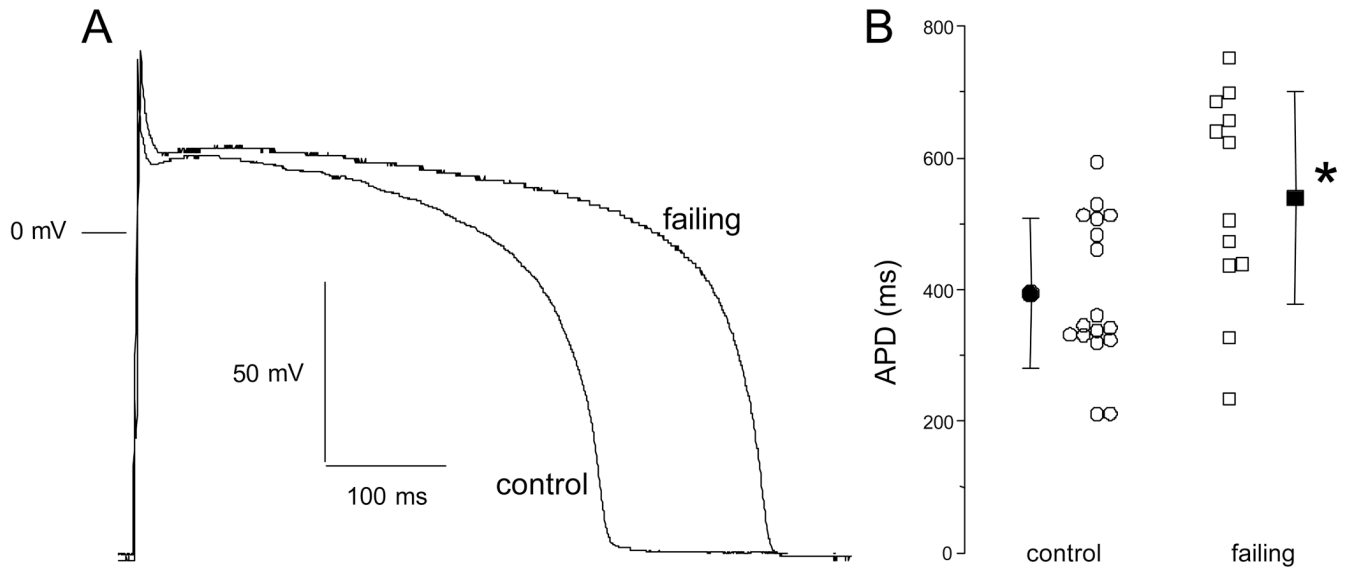

Figure 1.

Differences in the action potential shape and duration in ventricular myocytes isolated from control and failing ventricles. **A**. The action potential profile in a cell isolated from a failing heart is characterized by a longer duration compared to a cell isolated from a control heart. **B**. Summarized data for action potential duration at 90% repolarization (APD_{90}) in cells isolated from control (N=12 rabbits, n=17 cells) and failing (N=5 rabbits, n=12 cells) hearts. Despite a sizable variability, there is an overall prolongation of action potential duration in cells isolated from failing hearts. Mean±SD, *: $p<0.05$ vs. control.

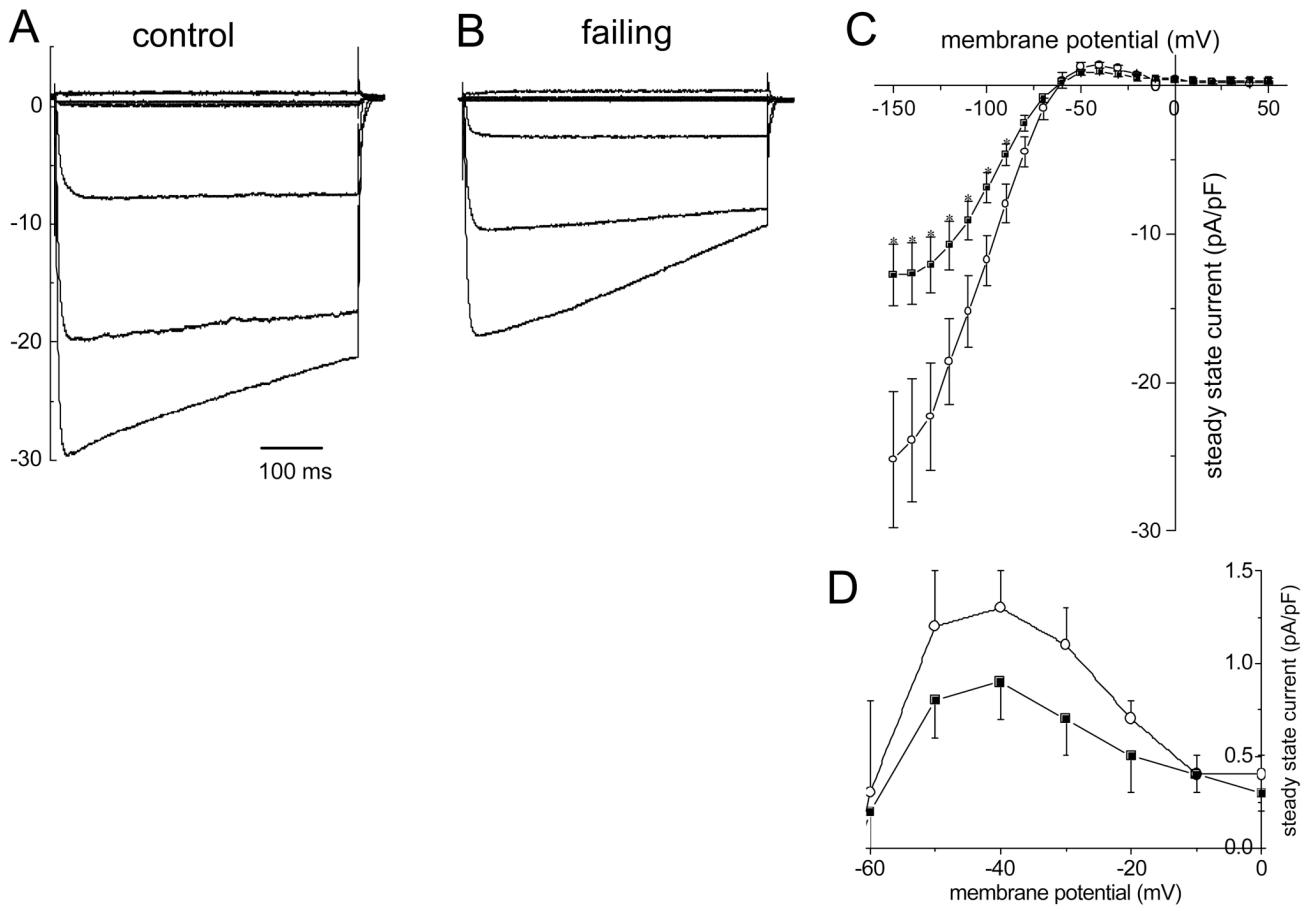

Figure 2.

Current density of inward rectifier current (I_{K1}) in ventricular myocytes isolated from control and failing ventricles. Representative families of currents recorded from a holding potential of −20 mV in response to voltage steps of 500 ms from −150 mV to 50 mV in 20 mV increments in cells isolated from control (**A**) and failing (**B**) myocardium. The tracings shown are Ba^{2+}-sensitive currents. The horizontal lines to the left of the current records indicate the zero-current level. **C**. The steady-state inward I_{K1} density is significantly reduced in cells isolated from failing (-■-, N=4 rabbits, n=8 cells) compared to cells isolated from control myocardium (-○-, N=4, n=9). **D**. The outward component of I_{K1} tends to decrease but the difference between cells isolated from control and failing hearts did not reach statistical significance. Mean ± SEM, *: $p<0.05$ vs. control.

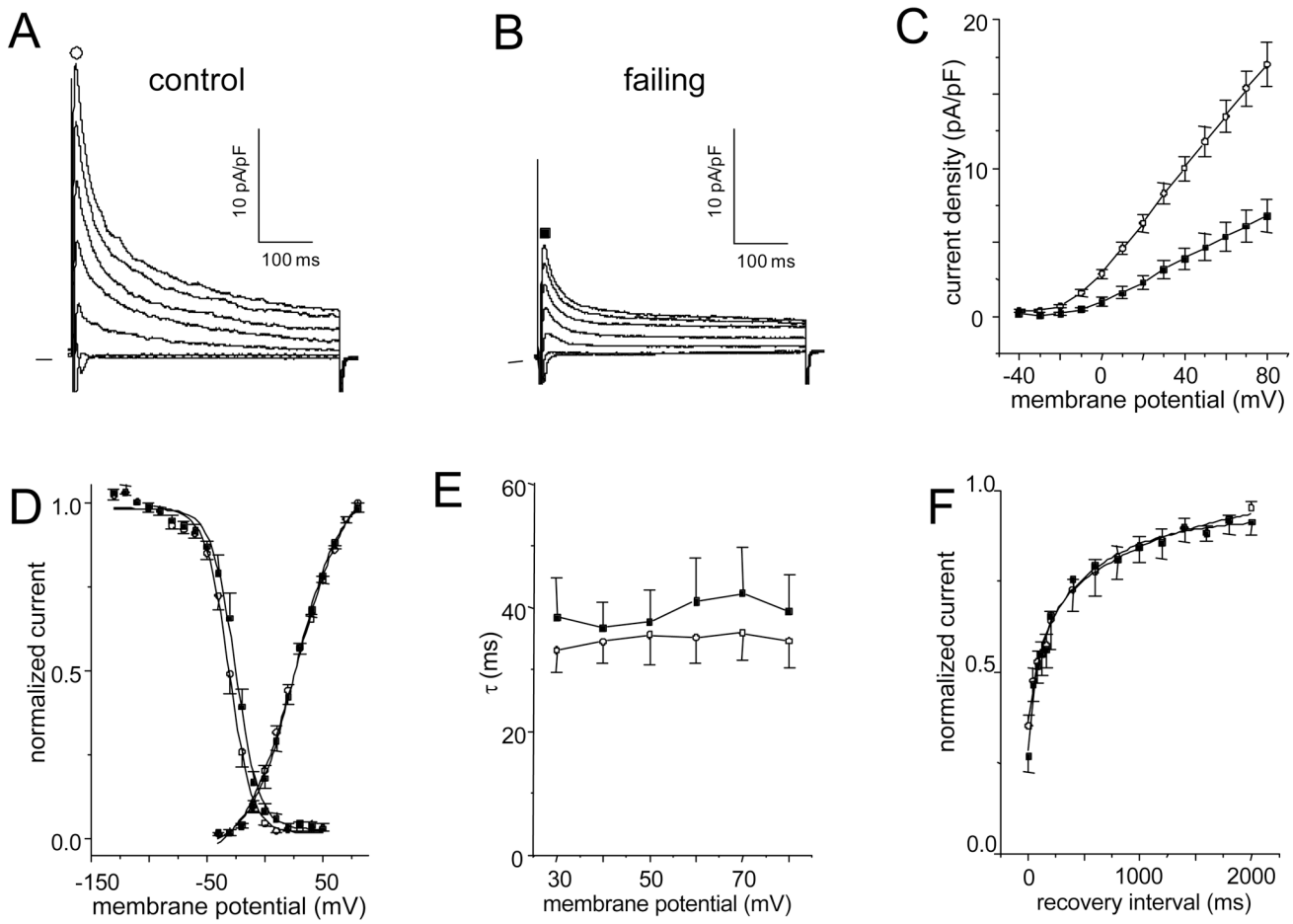

Figure 3.

Current density and kinetics of the calcium-independent transient outward current (I_{to}) in ventricular myocytes isolated from control and failing myocardium. Representative families of currents recorded from a holding potential of −80 mV in response to voltage steps of 500 ms from −40 mV to +80 mV in 20 mV increments in cells isolated from control (**A**) and failing (**B**) ventricles. The horizontal lines to the left of the current records indicate the zero-current level. **C**. The peak I_{to} density is significantly reduced in cells isolated from failing (-■-, N=11 rabbits, n=22 cells) compared to cells isolated from control myocardium (-○-, N=11, n=25). **D**. There was no difference in either the activation or the steady-state inactivation curves between cells isolated from control and failing myocardium. The fits to the data points are Boltzmann functions (control: -○-, N= 8, n=13, 27.3±1.8 mV half activation, 23.2±2.2 mV^{-1} maximal slope; N=6, n=7, −30.9±0.8 mV half inactivation, 9.9±0.7 mV^{-1} maximal slope; failing: -■-, N=7, n=10, 26.5±0.9 mV half activation, 19.1±1.0 mV^{-1} maximal slope; N=4, n=4, −25.3±1.0 mV half inactivation, 10.3±0.9 mV^{-1} maximal slope). **E**. There was no difference in the time constant of the macroscopic current relaxation (τ) between cells from control (-○-, N= 10, n= 20) and failing myocardium (-■-, N=5, n=11) determined by a single exponential fit of the first 150 ms of the current decay. **F**. Recovery from inactivation between cells from control (-○-, N=5, n=7, τ values of 120±45 ms and 1103±651 ms) and failing hearts (-■-, N=4, n=4, t values of 67±33 ms and 588±215 ms) did not differ. The lines were best fits to a biexponential function yielding the above-mentioned t. Mean ± SEM, *: $p<0.05$ vs. control.

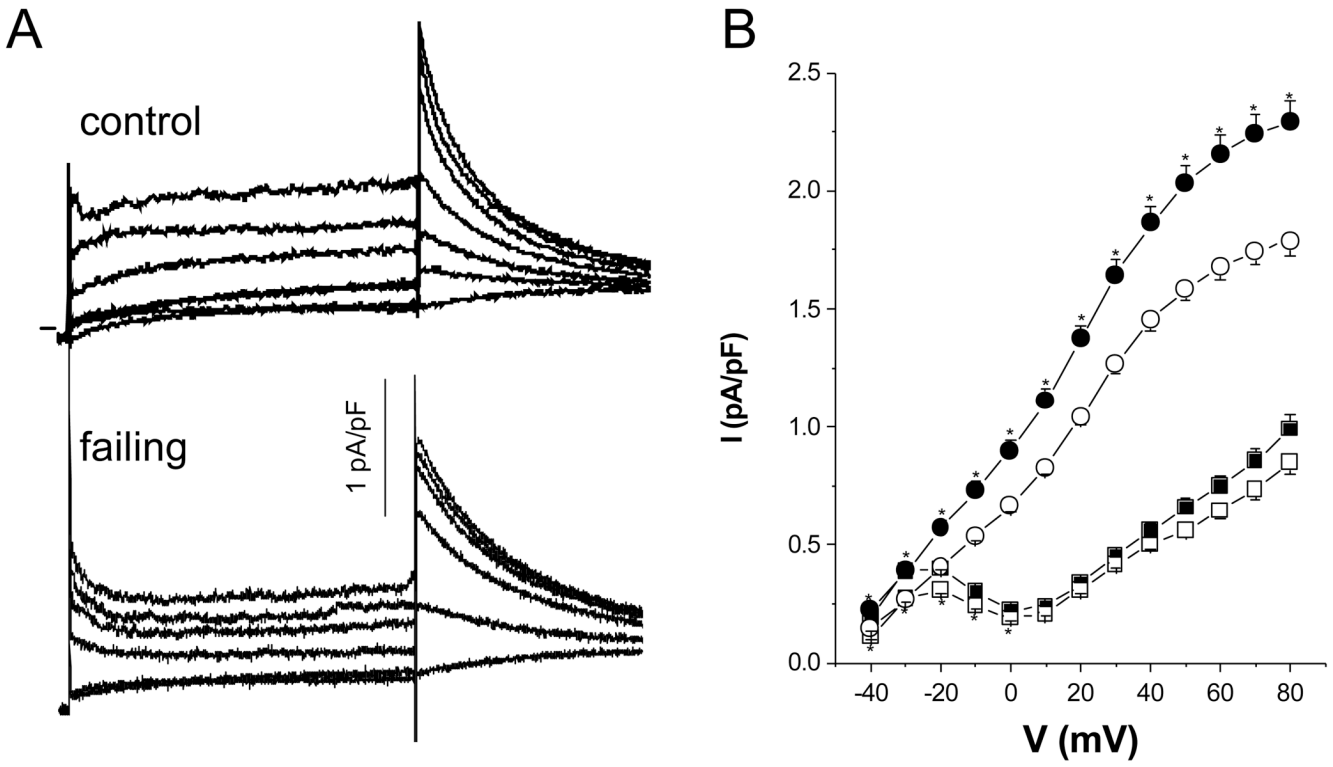

Figure 4.

A. Whole- cell I_K currents recorded in cells isolated from control and failing ventricles.. The cells are held at −80 mV and step currents are elicited by voltage pulses from −50 to 80 mV in increments of 10 mV for 3 seconds. Tail currents are measured on return to −30 mV. For clarity every other current trace is shown. The currents were recorded with 10 mM KCl in the extracellular solution. **B**. The step current is significantly reduced at negative voltages in cells isolated from failing (-□-, N=5 rabbits, n=36 cells) compared to cells isolated from control myocardium (-■-, N=6, n=38). The tail current is significantly reduced in cells isolated from failing (-○-, N=5 rabbits, n=36 cells) compared to cells isolated from control myocardium over the entire voltage range (-•-, N=6, n=38). Mean±SEM, *: $p<0.05$ vs. control.

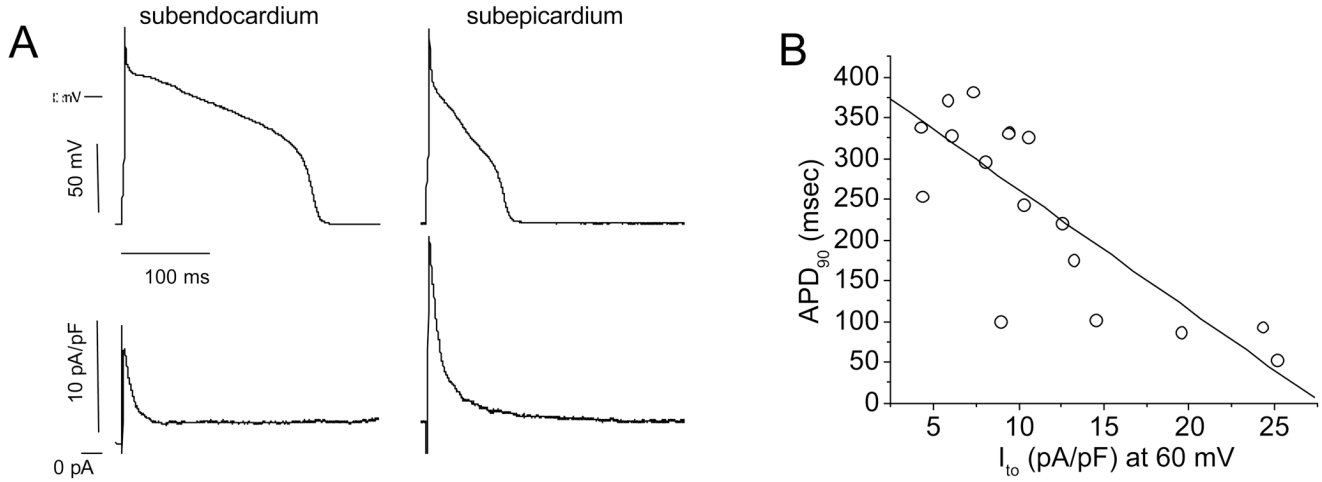

Figure 5.

Relationship between action potential duration and I_{to} density in rabbit left ventricular myocytes isolated from the subendocardial and subepicardial layers of the left ventricle. **A**. Action potential and I_{to} recordings at +60 mV in cells from the subendocardial and subepicardial layers of the left ventricle at 37 °C. The myocyte from the subendocardial layer was characterized by a long action potential duration and a moderate I_{to} density compared to the cell isolated from the subepicardial layer. **B**. A plot of the correlation between I_{to} density at +60 mV and action potential duration at 90 % repolarization (APD_{90}). There is a negative correlation between native I_{to} density and the APD_{90} ($y = -14.8x + 410$, $n = 18$, $r = -0.80$, $p < 0.05$), i.e. the higher the I_{to} density the shorter the action potential duration.

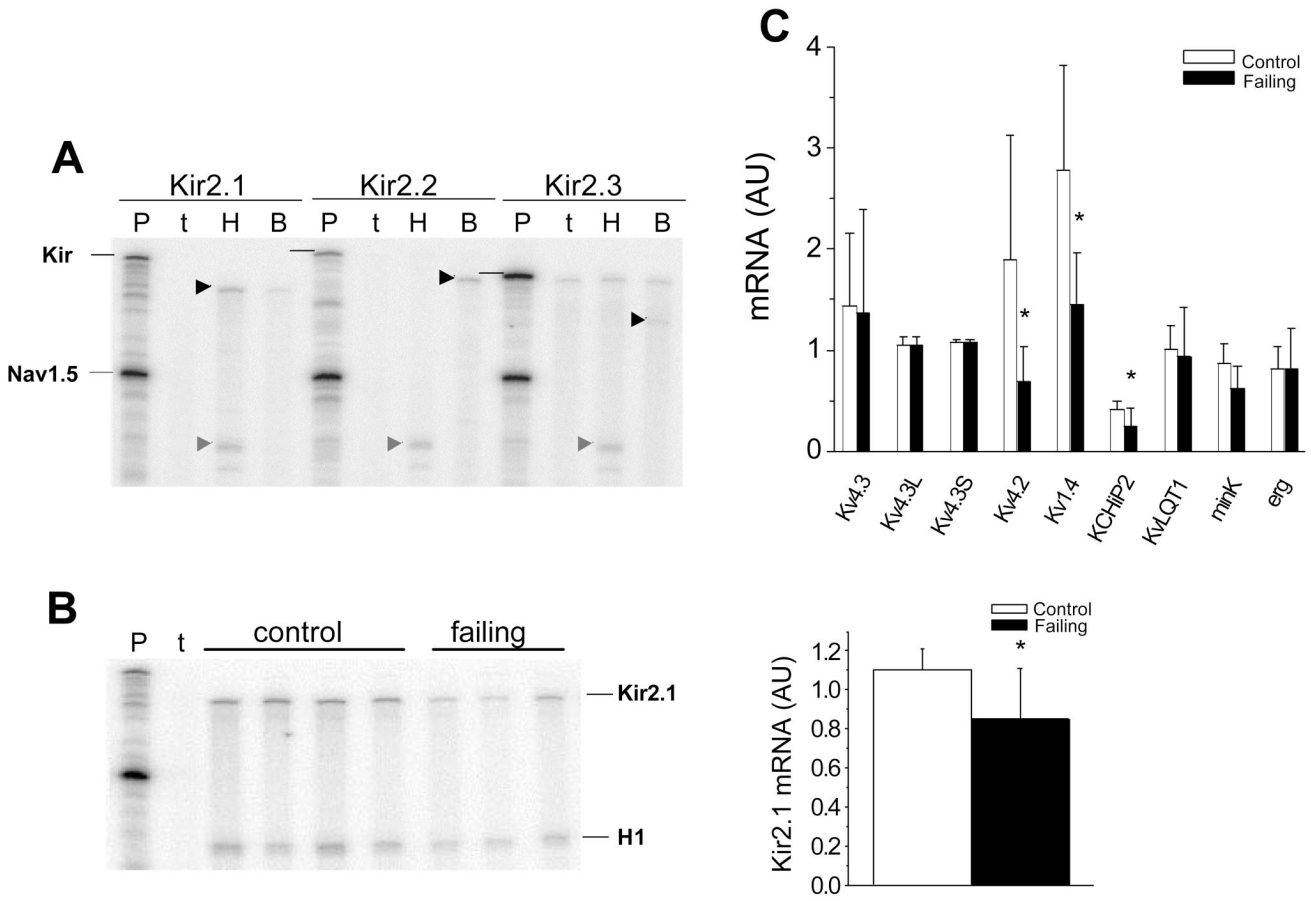

Figure 6.

mRNA levels of K channel subunits in the failing heart. (**A**). RPAs for Kir2.x mRNAs in rabbit heart and brain. The horizontal black lines identify the positions of the Kir2.x probes and the arrowheads represent the Kir2.x protected fragments. The abbreviations are P: probes, t: yeast tRNA; H: heart; B: brain. Only Kir2.1 is detected in rabbit ventricle, Kir2.1, Kir2.2 and Kir2.3 transcripts are detected in rabbit brain. **B**. A representative RPA measuring Kir2.1 in 4 control and 3 failing rabbit ventricles. A bar-plot demonstrating that steady-state Kir2.1 mRNA normalized to Nav1.5 is decreased in failing compared to control ventricles (N_c=10; N_f=10, p = 0.009). **C.** Real-time PCR quantification of steady-state mRNA for Kv4.3, Kv4.3L, Kv4.3S, (N_c=8; N_f=7, p = NS), Kv4.2 (N_c=8; N_f=7, p = 0.027), Kv1.4 (N_c=8; N_f=7, p = 0.0096), KChIP2 (N_c=9, N_f=9; p = 0.028), KvLQT1 (N_c=9, N_f=7; p = NS), minK (N_c=8; N_f=6, p = 0.055), Erg (N_c=8; N_f=7, p = NS) and RPA for Kir2.1 (N_c=10; N_f=10, p = 0.0093) normalized to 28S mRNA in control and failing rabbit ventricles (AU: Arbitrary Units).

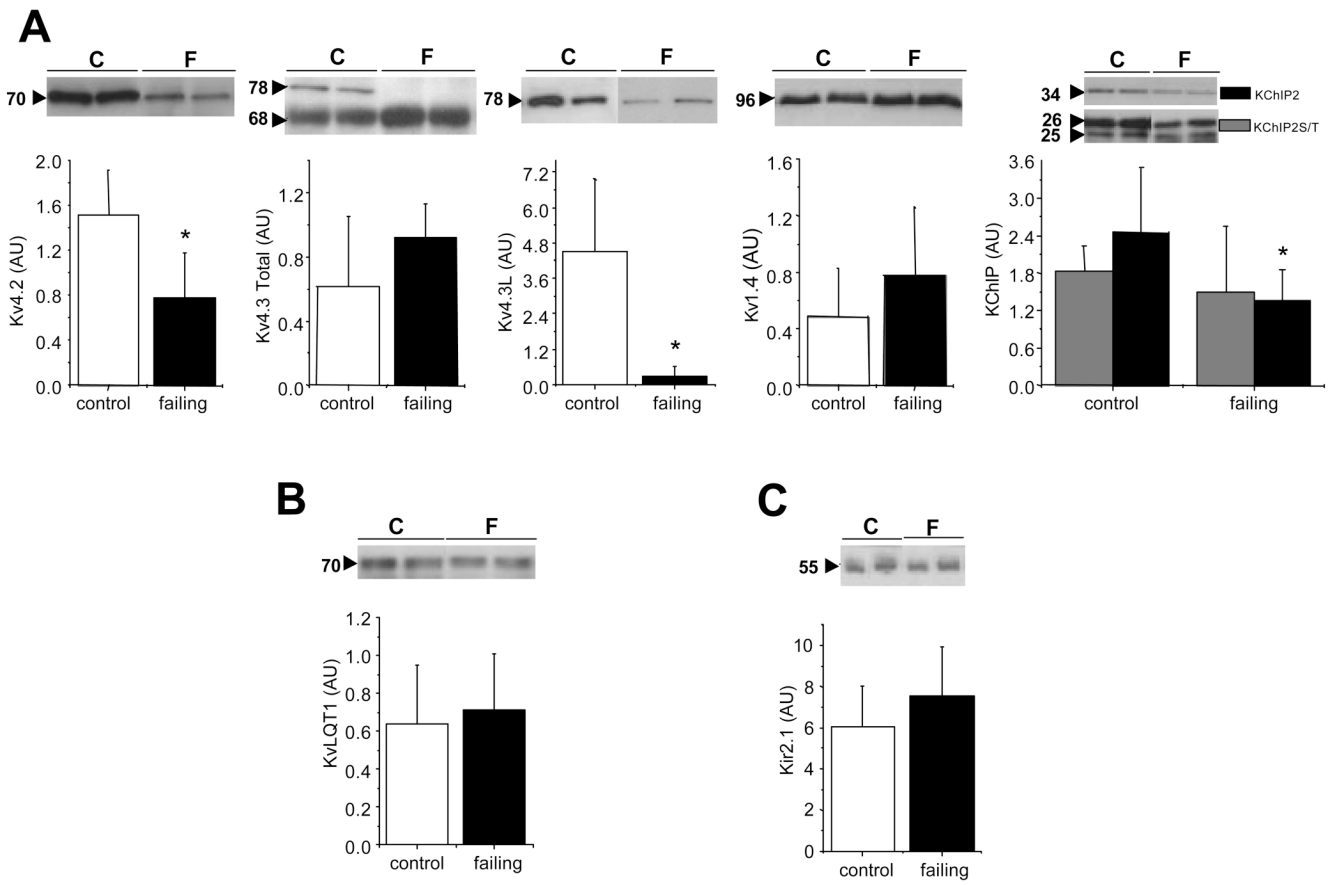

Figure 7.

Representative Western blots together with summary data for K channel subunits. **A**. Protein levels of putative I_{to} subunits. Antibodies to Kv4.2 exhibit a single major band at 70 kDa which was significantly decreased in failing hearts (N_c=6; N_f=5, $p < 0.05$). Two different anti-Kv4.3 antibodies were used, an antibody that recognizes total Kv4.3 exhibits two major bands at 78 and 68 kDa that were quantified (N_c=6; N_f=6; p = NS). The primary antibody was specific for the long splice variant, anti-Kv4.3L, recognized a single major band at 78 kDa that was significantly reduced in failing ventricles (N_c=8; N_f=8; p = 0.0003). Anti-Kv1.4 antibodies recognize a single band at 96 kDa that was unchanged in the failing hearts (N_c=12; N_f=10, p = NS). Two anti-KChIP antibodies were used, an antibody specific for KChIP2S/T isoforms reveals two bands at 25 and 26 kDa that were unchanged in the failing heart (N_c=4; N_f=8, p = NS). A pan-KChIP antibody recognizes a single major band at 34 kDa that was significantly decreased in the failing myocardium (N_c=7; N_f=7, $p < 0.05$). **B**. Delayed rectifier immunoreactive protein. Single bands at ~70 kDa were recognized with antibodies specific for KvLQT1 (N_c=10; N_f=11; p = NS), there was no significant change in failing hearts compared with controls. **C**. The anti-Kir2.1 antibody recognizes one band at 55 kDa that was unchanged in the failing hearts (N_c=6; N_f=8, p = NS). AU: Arbitrary Units.

Table 1

Characteristics of Pacing Heart Failure Model.

	Controls	Pacing Heart Failure	
N	**25**		**11**
		Baseline	**End Stage HF**
Days of pacing	—		20 ± 4
LV EDD (mm)	14.2 ± 3.2	12.8 ± 3.1	18.2 ± 4.8 *
Systolic FS (%)	41 ± 8	43 ± 7	24 ± 8 *
LV EDP (mmHg)	2.0 ± 3		19.0 ± 7.1 †
LV PPP (mmHg)	121 ± 4		97 ± 5 †
dP/dtmax (mmHg/s)	6900 ± 1620		3600 ± 270 †
HW/BW	0.00241 ± 4.13E-4		0.00297 ± 5.27E-4 †
LWW/BW	0.00133 ± 5.49E-4		0.00132 ± 5.93E-4

LV EDD: Left ventricular end diastolic diameter; FS: Fractional shortening; LV EDP: Left ventricular end diastolic pressure; LV PPP: peak pulse pressure; HW: heart weight; BW: body weight; LWW: lung wet weight

* $p < 0.05$ compared to baseline and controls;

† $p < 0.05$ compared to controls

Table 2

RPA and RT-PCR Primers and Probes

Transcript (accession #)	Probe/Primers
RPA	
Primers used to generate the respective RPA probes	
Kir2.1 (D21057)	
	forward 5’ AAT GCA GAC TTT GAA ATT GTT 3’
	reverse 5’ CTC TGG CAC TAC ACA GGG 3’
Kir2.2	
	forward 5’ CCA ACC CCT ACA GCA TCG 3’
	reverse 5’ TGA CCC AGA AGA TGA CAC C 3’
Kir2.3	
	forward 5’ ACA CAG CCG CAA CGG GCA GG 3’
	reverse 5’ AAC GGG CAC TCC TCT GTC ACA C 3’
H1 (Nav1.5)	nucleotides 1655 to 1801
	forward 5’ GGG AGA GCG AGA GCC ACC 3’
	reverse 5’ GTG GAC TGC AAT GGG GTG G 3’
RT-PCR	
Kv4.3 (AF198445)	probe 5’ 6FAMCGC CGA GCG CCT CAT GGATAMRA 3’
	forward 5’ AGG AGT ACA AGG ACC GCA AGA G 3’
	reverse 5’ GGT TGT TCT CCG AGT CGT TGT C 3’
Kv4.3L (AF198445)	probe 5’6FAMCCT GTT ATC TGT ACG AAC CTC CAC CAT CAATAMRA 3’
	forward 5’ CCA CTG GGT TGT CCT ATC TTG TG 3’
	reverse 5’ GTA GTT CTG CAT CGA GCT CTC CAT 3’
Kv4.3S (AF493549)	probe 5’ 6FAMCGC CTC ACT CAT CGA GAG CCA GCTAMRA 3’
	forward 5’ GAG GAG CAC ATG GGC AAG A 3’
	reverse 5’ TGA ACT CGT GGT TAG TGG TTT TCT C 3’
Kv4.2 (AF493547)	probe 5’ 6FAMTCT TCT CGC TCA CCATGG CCTAMRA 3’
	forward 5’ TCG GAG CTG GGC TTC TTG 3’
	reverse 5’ CGT AGA ACA TCA CTG TAG CAA AGA TG 3’
Kv1.4 (AJ291314)	probe 5’ 6FAMTGC TCT GAC CTG ATG CCC AGC GTAMRA 3’
	forward 5’ CAC CGA CAG AGC GGC TTT 3’,
	reverse 5’ CTC CCT TAG GAT CTT CTC CTC AGA 3’
Kchip	probe 5’ 6FAMCTG CAT CAC CAA GGA GGA AAT GCTTAMRA 3’
	forward 5’ TGA ATT GGG CCT TCA ACT TGT 3’,
	reverse 5’ GAT GTC GAG CAT TTC CTC CTT AG 3’
KvLQT1 (AJ291316)	probe 5’ 6FAMCCT GTA CAT CGG CTT CCT CGG CCTAMRA 3’
	forward 5’ CCG CCA GGA GCT GAT CAC 3’
	reverse 5’ TCT CAG CAG GTA CAC GAA GTA GGA 3’
minK (L41659)	probe 5’ 6FAMCGC TCT ACA TCC TCA TGG TGC TCG GTAMRA 3’
	forward 5’ GAC GAC GGG CAG ATG GAA 3’
	reverse 5’ ATG ATG CCC AGG GTG AAG AA 3’
erg (OCU97513)	probe 5’ 6FAMCTG GAC CAT CCT GCA TTA CAG CCTAMRA 3’
	forward 5’ CAG GCA CCA CGC ATC CA 3’

Transcript (accession #)	Probe/Primers
	reverse 5’ CAG TCC CAC ACA GCC TTG AA 3’